UDE-Based Robust Output Feedback Control With Applications to a Piezoelectric Stage

Beibei Ren, *Member, IEEE*, Jiguo Dai, *Student Member, IEEE*, and Qing-Chang Zhong, *Fellow, IEEE*

***Abstract*—In this article, an uncertainty and disturbance estimator (UDE)-based robust output feedback control technique without using a state observer is proposed for a general class of nonlinear single-input single-output systems that are bounded-input bounded-output stable and subject to input and output disturbances. Instead of designing a controller for the original system directly, an equivalent system consisting of a first-order linear system plus a lumped uncertainty term is used to represent the input–output relationship. Then, a UDE-based robust controller is designed only using the system output feedback and the bandwidth of the open-loop system, making the design almost modeling-free. A prominent advantage of the proposed approach is that it has converted a challenging robust control problem into an intuitive filter design problem. The effectiveness of the proposed approach is validated on an experimental piezoelectric stage in the presence of hysteresis nonlinearity.**

***Index Terms*—Hysteresis, output feedback, piezoelectric stage, trajectory tracking, uncertainty and disturbance estimator (UDE)-based robust control.**

I. Introduction

DEVELOPING robust control algorithms to achieve trajectory tracking and disturbance rejection is a vital goal of modern control theory. Among different robust control approaches, the uncertainty and disturbance estimator (UDE)-based robust control [1] has obtained much attention in recent years. It adopts a proper filter to estimate and compensate the lumped uncertainty, which may include the model uncertainties and external disturbances. This approach possesses a clear structure, easy tuning, and robust performance. Over the past years, it has been successfully applied to different applications, such as microelectromechanical systems [2], power systems [3], [4], industrial processes [5], unmanned aerial vehicles [6], [7], robotics [8], and distributed parameter systems [9]. In [10], its two-degree-of-freedom nature is revealed, decoupling the design of the reference model (to achieve the desired performance) and the design of a low-pass filter (to attenuate the effect of uncertainties and disturbances). Recently, the internal model principle has been introduced to systematically design the filter to achieve asymptotic performance [11].

Although a number of advancements have been made for the UDE-based robust control, there still exist some challenges. The first challenge comes from the structural constraint to be met by the original UDE-based robust controller for systems with the order greater than one [1]. The structural constraint elaborates that the lumped uncertainty should be "matched" with the control input, i.e., it should appear in the same channel of the control input [12]. Otherwise, the tracking performance can be degraded. The second challenge is that the original UDE-based robust control requires a full state feedback. In other words, all system states need to be measured for feedback, which is not the case in many applications. This motivates the development of an output feedback version of the UDE-based robust control in [13], where a controller–observer structure is proposed by constructing a Luenberger-like state observer to estimate the system states. However, the preferred performance can be guaranteed only when the lumped uncertainty varies slowly.

In this article, a UDE-based output feedback control framework without using a state observer is proposed for a general class of nonlinear single-input single-output (SISO) systems that are bounded-input bounded-output (BIBO) stable and subject to input disturbances and output disturbances. In order to facilitate the design, a first-order linear system is introduced to convert the original nonlinear system equivalently into a first-order linear system plus a lumped uncertainty term that consists of the original system dynamics and the opposite of the introduced first-order linear system. Then, the lumped uncertainty term is estimated through the UDE filter in the control design. A prominent advantage of the proposed approach lies in its almost modeling-free feature, as only the system output feedback and the bandwidth of the open-loop system are needed for the controller design. Moreover, the requirements of the structural constraint and the full state measurements are removed. This is very significant because it extends the applicability of the UDE-based robust control to a much larger class of systems. It does not matter whether the system is of a low order or of a high order. It does not matter whether the states of the system are available for measurement or not, either. It reduces the number of required sensors to the minimum, which reduces system cost.

Manuscript received January 27, 2019; revised June 15, 2019; accepted August 25, 2019. Date of publication September 19, 2019; date of current version April 30, 2020. This work was supported by the National Science Foundation under Grant CMMI-1728255. *(Corresponding author: Beibei Ren.)*

B. Ren and J. Dai are with the Department of Mechanical Engineering, Texas Tech University, Lubbock, TX 79409 USA (e-mail: beibei.ren@ttu.edu; jiguo.dai@ttu.edu).

Q.-C. Zhong is with the Department of Electrical and Computer Engineering, Illinois Institute of Technology, Chicago, IL 60616 USA (e-mail: zhongqc@ieee.org).

Color versions of one or more of the figures in this article are available online at http://ieeexplore.ieee.org.

Digital Object Identifier 10.1109/TIE.2019.2941169

There are many other excellent alternative robust control methods in the literature, e.g., [14]–[18]. Among them, proportional-integral-differential (PID) control is very popular, and it does not need the information of the system model. However, the tuning of the PID controller parameters is sometimes very challenging. Moreover, the scope of uncertainties a PID controller can handle may be limited. The superior performance of the UDE-based control over the PID has been discussed and demonstrated in [19]. In [14], a sliding-mode controller with a nonlinear disturbance observer (DOB) was proposed. This method requires state feedback. In [15], a higher order sliding-mode differentiation output feedback controller is studied to estimate the disturbances in nonlinear systems with any relative degree. In [16], an extended state observer (ESO) technique is applied to a hydraulic system with experimental validation. In [17], active disturbance rejection adaptive control is proposed to systems with unknown parameters. The output feedback model reference adaptive controller is studied for systems with time-varying state delays in [18]. In most of output feedback control design, a state observer (including an ESO) is constructed. This usually requires the information of system parameters and structure, which is a hassle and can be challenging for some applications. Instead of constructing a state observer, the proposed approach converts a challenging robust control problem into an intuitive filter design problem. It only requires the bandwidth of the open-loop system, which can be easily obtained through some preliminary studies of the system. Hence, one advantage is its significantly simplified design process, making it very attractive for practical applications.

In order to demonstrate its practical significance, the proposed approach is applied to control a piezoelectric nanopositioning stage, which can be widely found in microgrippers and scanning probe microscopes (SPMs) indispensable for investigating and manipulating nanoscale biological, chemical, material, and physical processes [20], [21]. It is crucial to achieve precise position control as well as high-bandwidth control for piezoelectric actuators, which would increase the operating speed of SPMs and bring significant benefits to numerous varieties of emerging nanosciences and nanotechnologies. However, the existence of vibration dynamics, coupled hysteresis, and other uncertainties, like creep, presents significant difficulties in the control of positioning and tracking over a wide bandwidth [22]. The currently commercially available high-resolution SPMs can only operate at a frequency range up to 1–10% of the lowest resonant frequency [22]. This motivated the development of control techniques to enable high-bandwidth nanopositioning and tracking of piezoelectric stages [23]–[26]. Compared to other approaches in the literature, the proposed approach can avoid complicated system modeling including hysteresis nonlinearity and lead to a simpler implementation, which requires less computational power. What is more important is that the presented control framework can achieve fine tracking up to 1100 Hz, which has reached 38% of the lowest resonant frequency, representing a significant improvement compared to the commercially available range of 1–10%.

The preliminary results of this article were presented in a conference paper [27]. New contributions of this journal version are highlighted as follows.

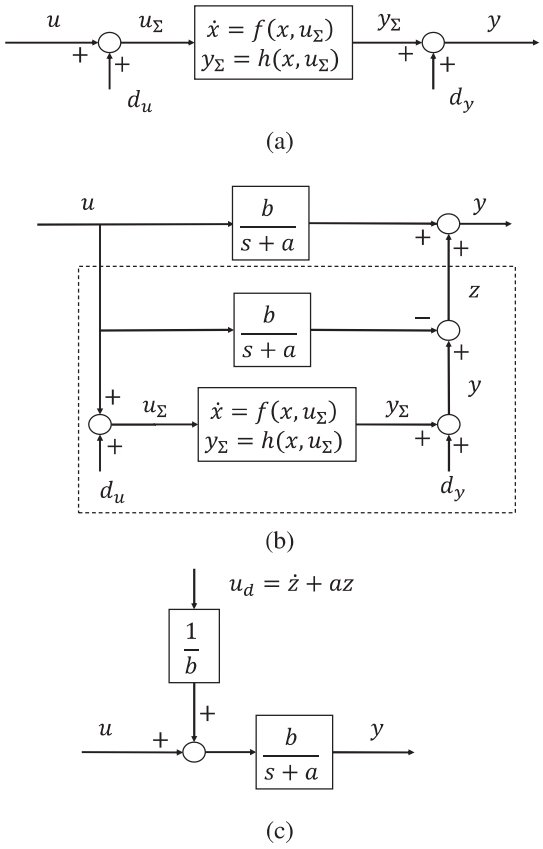

Fig. 1. System Σ in (a) and its equivalent transformations in (b) and (c).

1) The implementation of the proposed control framework has been redesigned to avoid internal instability issues caused by unstable pole-zero cancellation, as illustrated in Fig. 2.
2) The explicit conditions to guarantee the closed-loop system stability are analyzed and provided in Theorem 1 and its proof.
3) More details of the experimental validation are added, including experimental setup, system feasibility, and experimental results.
4) Comparisons with other works on the piezoelectric stage control are summarized to demonstrate the effectiveness of the proposed methodology.

The rest of this article is organized as follows. The problem is formulated in Section II with the main results presented in Section III. The application of the proposed approach to a piezoelectric stage is presented in Section IV. Section V concludes this article.

II. Problem Formulation

Consider the following general SISO nonlinear system, as shown in Fig. 1(a), with the input disturbance $d_u(t)$ and the output disturbance $d_y(t)$:

$$\Sigma: \begin{aligned} \dot{x}(t) &= f\left(x(t), u_\Sigma(t)\right) \\ y_\Sigma(t) &= h\left(x(t), u_\Sigma(t)\right) \end{aligned} \tag{1}$$

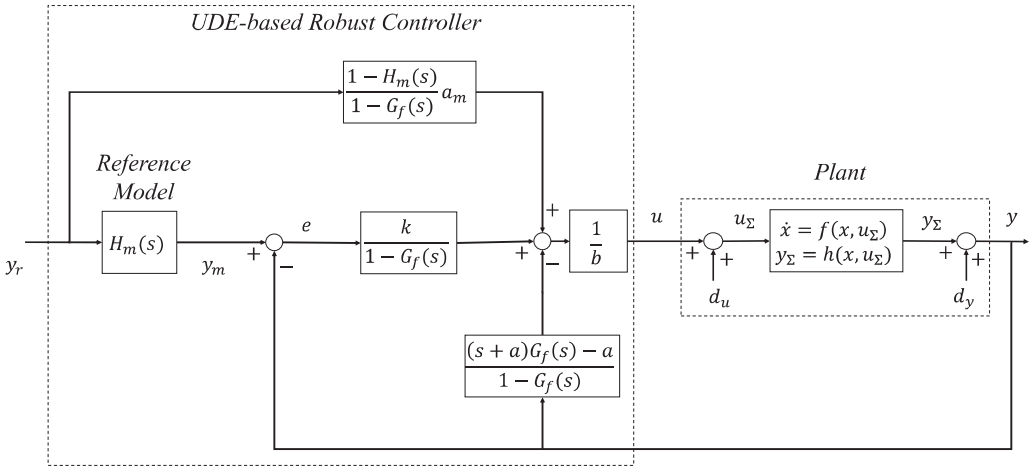

Fig. 2. Implementation of the proposed output feedback control.

where $x(t) \in \mathbb{R}^n$ is the state vector, $u_\Sigma(t) = u(t) + d_u(t) \in \mathbb{R}$, with $u(t)$ being the control input and $y(t) = y_\Sigma(t) + d_y(t) \in \mathbb{R}$ being the system output, $f(\cdot)$ is an unknown vector function, and $h(\cdot)$ is an unknown scalar differentiable function. The input–output relationship is denoted as $y_\Sigma(t) = \Sigma(u_\Sigma(t))$. Three assumptions are made for this system.

1) The system $\Sigma(\cdot)$ is BIBO with $\Sigma(u) = 0$ if and only if $u = 0$.
2) The system satisfies the Lipschitz condition $|\Sigma(u_1) - \Sigma(u_2)| \le \mu|u_1 - u_2|$, with $\mu = \|\Sigma\|_\infty$ being a positive number.
3) $d_u(t)$ and $d_y(t)$ are bounded. Without loss of generality, the bandwidth of the open-loop system is assumed to be ω_b rad/s.

In system (1), signals $x(t)$, $u_\Sigma(t)$, $y_\Sigma(t)$, $d_u(t)$, and $d_y(t)$ are unmeasurable or not measured, and only the system output $y(t)$ is measured for control design. The goal is to design a control law $u(t)$ to make the system output $y(t)$ track a desired reference signal $y_r(t) \in \mathbb{R}$. $y_r(t)$ is not necessarily continuous and can be smoothed after passing through a reference model $H_m(s)$ as $y_m(t)$. In order to simplify the exposition, the following first-order reference model is adopted:

$$\dot{y}_m(t) = -a_m y_m(t) + a_m y_r(t) \tag{2}$$

with $a_m > 0$ chosen to guarantee $y_m(t) = y_r(t)$ in the steady state. The control objective is then to design a control law $u(t)$ such that $y(t)$ tracks $y_m(t)$ fast and accurately, with the tracking error dynamics given as

$$\dot{e}(t) = -ke(t) \tag{3}$$

where $e(t) = y_m(t) - y(t)$ is the tracking error, and $k > 0$.

III. UDE-Based Robust Output Feedback Control

A. Control Framework

The system, as shown in Fig. 1(a), can be rearranged as shown in Fig. 1(b) after introducing a first-order linear system $\frac{b}{s+a}$, where $a > 0$, and the sign of b is the same as that of the system gain. Without loss of generality, $b > 0$ is considered in this article. The input–output relationship can be rewritten as

$$y(t) = \mathcal{L}^{-1}\left\{\frac{b}{s+a}\right\} * u(t) + z(t) \tag{4}$$

where "$*$" is the convolution operator, $\mathcal{L}^{-1}\{\cdot\}$ is the inverse Laplace operator, and

$$z(t) = y(t) - \mathcal{L}^{-1}\left\{\frac{b}{s+a}\right\} * u(t).$$

From (4), there is

$$\dot{y}(t) = -ay(t) + bu(t) + u_d(t) \tag{5}$$

as shown in Fig. 1(c), where

$$u_d(t) = \dot{z}(t) + az(t) \tag{6}$$

is a lumped uncertainty, including the original system dynamics and the opposite of the introduced first-order linear system. It is worth highlighting that representing the original system (1) in (5) with a first-order linear system plus the lumped uncertainty term (6) does not introduce any error. Moreover, the selection of the parameters of the first-order linear system is straightforward, as will be shown later. The introduction of the first-order linear system is purely to facilitate the design of the control law. Subtracting (5) from (2) results in

$$\begin{aligned}\dot{e}(t) = \; & -ke(t) + [ke(t) - a_m y_m(t) + a_m y_r(t) \\ & + ay(t) - bu(t) - u_d(t)]. \end{aligned} \tag{7}$$

In order to satisfy the error dynamics (3), the controller should satisfy

$$u(t) = \frac{1}{b}\left[-a_m y_m(t) + a_m y_r(t) + ke(t) + ay(t) - u_d(t)\right]. \tag{8}$$

Everything on the right-hand side of the equation is known, except the lumped uncertainty $u_d(t)$ that can be rewritten, according to (5), as

$$u_d(t) = \dot{y}(t) + ay(t) - bu(t).$$

According to the UDE-based robust control strategy [1], it can be estimated as

$$\hat{u}_d(t) = g_f(t) * u_d(t) = g_f(t) * (\dot{y}(t) + ay(t) - bu(t)) \quad (9)$$

where $g_f(t) = \mathcal{L}^{-1}\{G_f(s)\}$ is the impulse response of a strictly proper and stable filter $G_f(s)$ with the unity gain and zero phase shift over the bandwidth of the open-loop system and zero gain elsewhere. In practice, its bandwidth, denoted as ω_f, can be much wider than the open-loop system bandwidth ω_b. By replacing $u_d(t)$ in (8) with $\hat{u}_d(t)$ in (9), the UDE-based robust output feedback controller can be derived as

$$u(t) = \frac{1}{b}\left[ay(t) - \mathcal{L}^{-1}\left\{\frac{sG_f(s)}{1-G_f(s)}\right\} * y(t) + \mathcal{L}^{-1}\left\{\frac{1}{1-G_f(s)}\right\} * (-a_m y_m(t) + a_m y_r(t) + ke(t))\right]. \quad (10)$$

This leads to the overall control structure, which can be implemented, as shown in Fig. 2. Compared to the results in [27], the implementation in Fig. 2 avoids possible internal instability issues caused by unstable pole-zero cancellation. Normally, $H_m(s)$ and $G_f(s)$ have a unity static gain, which means $H_m(0) = 1$ and $G_f(0) = 1$. Hence, there is an integrator in $\frac{1}{1-G_f(s)}$, and there is a differentiator in $1 - H_m(s)$. If these two blocks are implemented separately as in [27], there is a pole-zero cancellation at $s = 0$, which leads to an internal instability problem. The implementation in Fig. 2 can avoid this via implementing $\frac{1-H_m(s)}{1-G_f(s)}$ as a whole after canceling the zero and pole at $s = 0$.

B. Stability Analysis

After rearranging the blocks in Fig. 2 and representing the plant by its equivalent representation in Fig. 1(b), the closed-loop system shown in Fig. 2 can be expressed as shown in Fig. 3(a), where

$$G_1(s) = a_m - \frac{a_m^2}{s+a_m} + \frac{a_m k}{s+a_m} = \frac{a_m(s+k)}{s+a_m} \quad (11)$$

$$G_2(s) = \frac{1}{1-G_f(s)} \quad (12)$$

$$G_3(s) = k + sG_f - a(1-G_f) = (k-a) + (s+a)G_f \quad (13)$$

and $d(t)$ represents the effect of $d_u(t)$ and $d_y(t)$ given by

$$d(t) = \Sigma(u(t) + d_u(t)) - \Sigma(u(t)) + d_y(t).$$

The dashed block Δ in Fig. 3(a) characterizes the deviation of the introduced first-order linear system from the original system.

Theorem 1: For the nonlinear BIBO system $y_\Sigma(t) = \Sigma(u_\Sigma(t))$ described in (1) with bounded disturbances $d_u(t)$ and $d_y(t)$ and open-loop system bandwidth ω_b rad/s, the closed-loop system described in Fig. 2, which involves the reference model (2) and the control law (10), is finite-gain $\mathcal{L}_\infty$ stable [1] if: i) the first-order linear system $\frac{b}{s+a}$ is chosen with $a = \eta\omega_b$, where $\eta \gg 1$, and $b = k_s a$, where $k_s > \frac{\sqrt{1+\eta^2}}{\eta}\mu$; ii) the UDE-filter satisfies $\|G_f(s)\|_\infty = 1$, and iii) the error dynamics gain $k > a$.

[1] A system $\hat{\Sigma}: \mathbb{R} \to \mathbb{R}$ is said to be finite-gain $\mathcal{L}_\infty$ stable, if there exist nonnegative constants γ and β such that $\|\hat{\Sigma}u\|_{\mathcal{L}_\infty} \le \gamma\|u\|_{\mathcal{L}_\infty} + \beta$ [28].

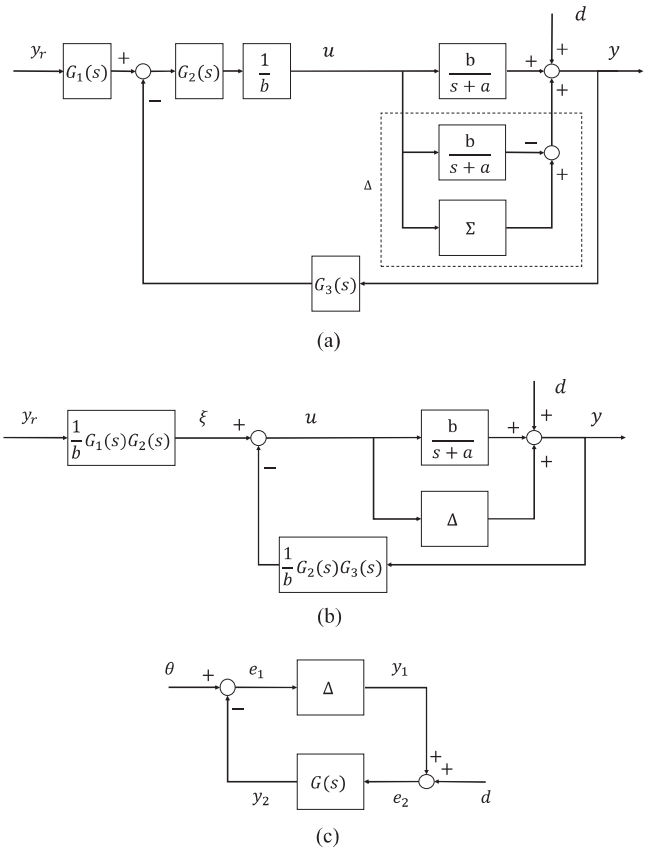

Fig. 3. Equivalent representations of the UDE-based robust output feedback control system in Fig. 2 for analysis.

Proof: The closed-loop system shown in Fig. 3(a) can be represented as Fig. 3(b) and (c) to facilitate the analysis. Fig. 3(c) illustrates the feedback connection between $\Delta = \Sigma - \frac{b}{s+a}$ and a linear part $G(s)$, where

$$G(s) = \frac{\frac{1}{b}G_2(s)G_3(s)}{1 + \frac{1}{s+a}G_2(s)G_3(s)} \quad (14)$$

$$\theta(t) = \mathcal{L}^{-1}\left\{\frac{\frac{1}{b}G_1(s)G_2(s)}{1 + \frac{1}{s+a}G_2(s)G_3(s)}\right\} * y_r(t)$$

$e_1(t) = u(t)$, $y_1(t) = \Delta \cdot e_1(t)$, $e_2(t) = y_1(t) + d(t)$, and $y_2(t) = \mathcal{L}^{-1}\{G(s)\} * e_2(t)$. According to assumptions 2) and 3), $\theta(t)$ and $d(t)$ are bounded. Applying (12) and (13) into (14) results in

$$G(s) = \frac{(s+a)^2 G_f(s) + (k-a)s + a(k-a)}{b(s+k)}. \quad (15)$$

Since $G_f(s)$ is stable and $k > 0$, $G(s)$ is asymptotically stable. Moreover, $G(s)$ is proper because $G_f(s)$ is a low-pass filter. Hence, $G(s)$ is bounded on the right half s-plane and has a finite ∞ norm.

According to the BIBO assumption about the system $\Sigma(\cdot)$, $\mu = \|\Sigma\|_\infty$ exists, and the bandwidth ω_b of the system is known. Once the parameters are chosen to satisfy the conditions i)–iii), the following estimations can be made.

The ∞ norm of Δ can be estimated as $\gamma_1 = \|\Delta\|_\infty \leq (\eta k_s/\sqrt{1+\eta^2} - \epsilon)$, where $0 < \epsilon \leq \mu$. Furthermore, the ∞ norm of $G(s)$ can be estimated as $\gamma_2 = \|G\|_\infty \leq \|\frac{(s+a)^2 G_f(s)}{b(s+k)}\|_\infty + \|\frac{(k-a)s+a(k-a)}{b(s+k)}\|_\infty \leq \frac{k+\omega_b(\sqrt{1+\eta^2}-\eta)}{k_s \eta \omega_b}$. Therefore, let $\eta \to \infty$ and $k = \eta\omega_b + \phi \geq a$, where $\phi \geq 0$; there is

$$\gamma_1\gamma_2 = \left(\frac{\eta}{\sqrt{1+\eta^2}}k_s - \epsilon\right)\frac{\eta\omega_b + \phi + \omega_b\left(\sqrt{1+\eta^2}-\eta\right)}{k_s\eta\omega_b} \approx \frac{k_s-\epsilon}{k_s} < 1. \tag{16}$$

Hence, according to the small-gain theorem [28], this feedback connection is finite gain $\mathcal{L}_\infty$ stable. This completes the proof. ■

This theorem indicates that all the signals $(e_1(t), y_1(t), e_2(t), y_2(t))$ in Fig. 3(c) are bounded under the conditions. Both $\theta(t)$ and $d(t)$ are bounded based on the boundedness of $e_1(t)$, $y_r(t)$, $d_u(t)$, and $d_y(t)$. The system output is

$$y(t) = \mathcal{L}^{-1}\left\{\frac{b}{s+a}\right\} * e_1(t) + e_2(t)$$

which is also bounded.

C. Asymptotic Convergence Analysis

As discussed before, the closed-loop system can be equivalently represented, as shown in Fig. 3(a) and (b), which include a block $G_2(s) = \frac{1}{1-G_f(s)}$, as given in (12). According to the internal model principle, in order to guarantee that the tracking error converges to 0 asymptotically, i.e., $\lim_{t\to\infty} e(t) = 0$, the filter $G_f(s)$ can be designed in such a way that $G_2(s)$ includes the generation models of the reference command $y_r(t)$ and the disturbances $d_u(t)$ and $d_y(t)$. The details about this can be found in [11]. For example, when there exist harmonic components at frequencies $n\omega$ and the step signals in the system, the following filter can be used:

$$G_f(s) = 1 - \frac{s\prod_n(s^2 + (n\omega)^2)}{(s+\alpha)\prod_n(s^2 + \alpha_n s + \beta_n)} \tag{17}$$

where α, α_n, and β_n are positive design parameters [11]. This guarantees that $G_f(s)$ has the unity gain and zero phase shift at the frequencies $n\omega$.

In the following, the actual tracking error is analyzed. Denote the Laplace transform of a signal with a capitalized letter, e.g., $Y(s)$ and $U_d(s)$ are the Laplace transforms of $y(t)$ and $u_d(t)$, respectively. After taking the Laplace transform, the system (5) becomes

$$sY(s) = -aY(s) + bU(s) + U_d(s) \tag{18}$$

the reference model (2) becomes

$$sY_m(s) = -a_m Y_m(s) + a_m Y_r(s) \tag{19}$$

and the controller (10) becomes

$$bU(s) = -a_m Y_m(s) + a_m Y_r(s) + kE(s) + aY(s) - U_d(s)G_f(s) \tag{20}$$

according to (8) and (9). Combining (18)–(20) results in

$$sE(s) = -kE(s) - U_d(s)\left[1 - G_f(s)\right] \tag{21}$$

which indicates that the actual error dynamics is

$$E(s) = -\frac{1}{s+k}\left[1 - G_f(s)\right]U_d(s). \tag{22}$$

As a result, the lumped uncertainty signal $u_d(t)$ is attenuated twice, first by a low-pass filter $\frac{1}{s+k}$ and then by a frequency-selective high-pass filter $1 - G_f(s)$. The high-frequency components of $u_d(t)$, such as measurement noises, are attenuated by the low-pass filter, and the low-frequency components of $u_d(t)$ are attenuated by the high-pass filter after passing through the low-pass filter. Hence, the functions of these two filters are decoupled in the frequency domain, similar to the case in [10]. When $G_2(s)$ is designed to include the generation models of the reference command $y_r(t)$ and the disturbances $d_u(t)$ and $d_y(t)$, it is equivalent for $1 - G_f(s)$ to have zero gain at the corresponding modes (frequencies). As a result, the contribution of the reference command $y_r(t)$ and the disturbances $d_u(t)$ and $d_y(t)$ will eventually converge to zero. In other words, the actual tracking error will asymptotically converge to zero.

For a required attenuation ratio $\delta > 0$ over the bandwidth of the system, the design should guarantee

$$\left|\frac{1 - G_f(j\omega)}{j\omega + k}\right| \leq \delta. \tag{23}$$

D. Achievable Control Bandwidth of the Closed-Loop System

According to the definition of the tracking error in (3) and the actual tracking error in (22), the system output is

$$Y(s) = H_m(s)Y_r(s) - E(s) = \frac{a_m}{s+a_m}Y_r(s) + \frac{1}{s+k}\left[1 - G_f(s)\right]U_d(s).$$

According to the analysis in the previous subsection, the tracking error $e(t)$ converges to zero. Moreover, the bandwidth ω_f of the UDE filter $G_f(s)$ and the error dynamics gain k can be chosen to be much larger than a_m. In this way, the error $e(t)$ converges to zero faster than the reference output $y_m(t)$ converges to the reference input $y_r(t)$. As a result, the closed-loop system response is dominated by the reference model. In other words, the bandwidth of the closed-loop system is the bandwidth of the reference model, which is $\omega_c = a_m$ for the reference model $H_m(s) = \frac{a_m}{s+a_m}$ selected in (2).

IV. Application to Piezoelectric Stage Control

In this section, the effectiveness of the proposed control approach is demonstrated on a piezoelectric actuator experimental platform. The tracking performance of piezoelectric actuator can

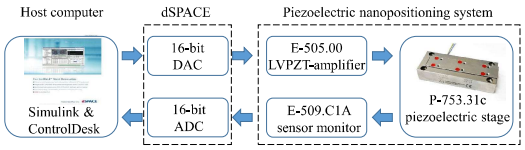

Fig. 4. Experimental setup.

TABLE I
SYSTEM PARAMETERS

Module	Parameter	Value*	Unit
E-505.00	Control input	-2 to 12	V
	DC-offset to control input	0 to 10	V
	Voltage gain	10±0.1	-
	Output voltage	-30 to 130	V
P-753.31c	Mass	250	g
	Nominal expansion	38	μm
	Unloaded resonant frequency	2.9±20%	kHz
	Stiffness in motion direction	16±20%	$N/\mu m$
	Full-range repeatability	±3	nm
E-509.C1A	Output	0 to 10	V
	Sensitivity	3.8	$\mu m/V$
	Resolution	0.2	nm
	Bandwidth	3	kHz
	Linearity	0.05%	-

* from http://www.pi.ws

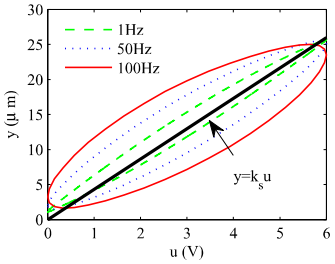

Fig. 5. Major hysteresis loops resulted from sinusoidal signals $u(t) = 3(\sin(2\pi ft) + 1)$V at different frequencies $f = 1$ Hz, 50 Hz, 100 Hz. u is the input voltage and y is the output displacement.

be pushed to the hardware limit in the sense of high precision and high bandwidth.

A. Experimental Setup and System Information

Fig. 4 shows the experimental setup, including a piezoelectric nanopositioning system from Physik Instrumente GmbH & Co. KG, a dSPACE-DS1104 board, and a host computer. In the piezoelectric nanopositioning system, the piezoelectric stage P-753.31c, of which the maximum displacement is 38 μm from its static equilibrium point, is driven by a linear voltage amplifier E-505.00 with a fixed gain of 10 to amplify the control signal from dSPACE. Then, its real-time displacement is measured by an integrated capacitive sensor and transferred to analog voltage via the sensor monitor E-509.C1A. The detailed specification of the piezoelectric nanopositioning system is listed in Table I. Moreover, the sampling time adopted in the experiment is 0.01 ms. The resolution of this system is around 0.0012 μm.

Fig. 5 shows the major hysteresis loops resulting from the sinusoidal inputs $u(t) = 3(\sin(2\pi ft) + 1)$V at different frequencies $f = 1$ Hz, 50 Hz, 100 Hz, where $y = k_s u$ is the approximated axis of symmetry of hysteresis loops.

Different models have been proposed to characterize the rate-dependent hysteresis, as shown in [29]–[32]. The rate-dependent Prandtl–Ishlinskii hysteresis model in [29] can be utilized in the piezoelectric stage. To formulate the rate-dependent Prandtl–Ishlinskii hysteresis model, the rate-dependent play operator, $w(t) = F_{r_i(\dot{u})}[u](t) = f_{r_i(\dot{u})}(u(t),\ F_{r_i(\dot{u})}[u](t_{j-1}))$, with dynamic threshold $r_i(\dot{u}) > 0$, is first defined as

$$F_{r_i(\dot{u})}[u](0) = f_{r_i(\dot{u})}(u(0),\ 0)$$
$$f_{r_i(\dot{u})}(u,\ w(t_{j-1})) = \begin{cases} \max(u(t) - r_i(\dot{u}), w(t_{j-1})), & u(t) > u(t_{j-1}) \\ \min(u(t) + r_i(\dot{u}), w(t_{j-1})), & u(t) < u(t_{j-1}) \\ w(t_{j-1}), & u(t) = u(t_{j-1}) \end{cases}$$
$$\text{for } t_{j-1} < t \le t_j \text{ and } 1 \le j \le \bar{M} \tag{24}$$

where $u(t) \in AC[0,\ t_E]$ is the input voltage, with $AC[0,\ t_E]$ representing the space of absolutely continuous functions on the time interval $[0,\ t_E]$. $0 = t_0 < t_1 < \cdots < t_{\bar{M}} = t_E$ is partition of $[0,\ t_E]$, and the function $u(t)$ is monotone on each of the subintervals $(t_j,\ t_{j+1}]$. The argument of the operator, which is written in square brackets, indicates the functional dependence, since it maps a function to a function. Similar to the rate-independent Prandtl–Ishlinskii hysteresis model that is constructed by the superposition of weighted play operators with different thresholds, the rate-dependent Prandtl–Ishlinskii model can be formulated as follows [29]:

$$y(t) = H[u](t) = a_0 u(t) + \sum_{i=1}^{N} a_i F_{r_i(\dot{u})}[u](t) \tag{25}$$

where $y(t)$ is the system output displacement, a_i, $i = 0,\ 1,\ 2, \ldots,\ N$, are positive weights, and N is the total number of rate-dependent play operators. It should be noted that the dynamic thresholds $r_i(\dot{u})$ need to satisfy $0 \le r_1(\dot{u}) \le r_2(\dot{u}) \le \cdots \le r_N(\dot{u})$. Specifically, $r_i(\dot{u}) = \alpha_i + g(\dot{u}) = \zeta i + \beta|\dot{u}|$ from [29] is utilized in this article.

B. System Feasibility

The studied system should be verified to satisfy the BIBO assumption and Lipschitz condition mentioned in Section II.

Lemma 2: If the reference trajectory $y_r(t)$ is Lipschitz continuous, then the UDE-based robust controller (10) generates an absolutely continuous control signal $u(t)$.

Proof: Since both $\mathcal{L}^{-1}\{\frac{sG_f(s)}{1-G_f(s)}\}$ and $\mathcal{L}^{-1}\{\frac{1}{1-G_f(s)}\}$ are continuous operators, and $y_r(t)$ and $y_m(t)$ are continuous signals, then the control input $u(t)$ is a continuous signal. Moreover, $y(t)$ is a Lipschitz continuous signal, since the generalized Prandtl–Ishlinskii model is Lipschitz continuous [33]. Consequently, $u(t)$ is also a Lipschitz continuous signal and thus absolutely continuous. ■

Proposition 3: The hysteresis system (25) is BIBO and satisfies the Lipschitz condition.

Proof: According to Lemma 2, $u(t)$ is absolutely continuous, which satisfies the condition in the rate-dependent Prandtl–Ishlinskii model. And from (24), if $u(t) > u(t_{j-1})$, i.e., $\dot{u}(t) > 0$, then $f_{r_i(\dot{u})}(u, w) = \max(u - r_i(\dot{u}), w) \geq u(t) - r_i(\dot{u})$. Therefore, $F_{r_i(\dot{u})}[u](t) \geq u(t) - r_i(\dot{u})$. Hence, from (25), we have

$$\begin{aligned} y(t) &= a_0 u(t) + \sum_{i=1}^{N} a_i F_{r_i(\dot{u})}[u](t) \\ &\geq a_0 u(t) + \sum_{i=1}^{N} a_i (u(t) - r_i(\dot{u})) \\ &= u(t) \sum_{i=0}^{N} a_i - \sum_{i=1}^{N} a_i (\zeta i + \beta |\dot{u}|) \\ &\geq u(t) \sum_{i=0}^{N} a_i - \sum_{i=1}^{N} a_i (\zeta N + \beta \max(|\dot{u}|)) \\ &= u(t) \sum_{i=0}^{N} a_i - (\zeta N + \beta \max(|\dot{u}|)) \sum_{i=1}^{N} a_i \\ &= \rho u(t) - D_H \end{aligned}$$

where $\rho = \sum_{i=0}^{N} a_i$, and $D_H = (\zeta N + \beta \max(|\dot{u}|)) \sum_{i=1}^{N} a_i$.

Similarly, if $u(t) < u(t_{j-1})$, i.e., $\dot{u}(t) < 0$, then $f_{r_i(\dot{u})}(u, w) = \min(u + r_i(\dot{u}), w) \leq u(t) + r_i(\dot{u})$. Therefore, $F_{r_i(\dot{u})}[u](t) \leq u(t) + r_i(\dot{u})$. Hence, from (25), we have

$$\begin{aligned} y(t) &= a_0 u(t) + \sum_{i=1}^{N} a_i F_{r_i(\dot{u})}[u](t) \\ &\leq a_0 u(t) + \sum_{i=1}^{N} a_i (u(t) + r_i(\dot{u})) \\ &= u(t) \sum_{i=0}^{N} a_i + \sum_{i=1}^{N} a_i (\zeta i + \beta |\dot{u}|) \\ &\leq u(t) \sum_{i=0}^{N} a_i + \sum_{i=1}^{N} a_i (\zeta N + \beta \max(|\dot{u}|)) \\ &= u(t) \sum_{i=0}^{N} a_i + (\zeta N + \beta \max(|\dot{u}|)) \sum_{i=1}^{N} a_i \\ &= \rho u(t) + D_H. \end{aligned}$$

Therefore, there always exists $\|y(t)\| \leq \rho \|u(t)\| + D_H$. And the Lipschitz condition can be easily verified. This completes the proof. ■

C. Control Design

The reference signal is chosen as $y_r(t) = 1 + \sin(\omega t - \pi/2)\mu$m, where $\omega = 2\pi f$ represents the operating frequency of the piezoelectric stage, with $f \in [1\,\text{Hz},\ 2500\,\text{Hz}]$. The reference model (2) is selected as $\frac{a_m}{s+a_m} = \frac{50\,000\pi}{s+50\,000\pi}$ with a bandwidth $a_m = 50\,000\pi$. This bandwidth is around ten times greater than the maximum operating frequency, 2500 Hz, which is sufficient to obtain a good reference state $y_m(t)$. The first-order system is chosen as $\frac{b}{s+a}$, where $a = 60\,000\pi$ and $b = 260\,000\pi$. The ratio $b/a = k_s$, which is the approximated slope in Fig. 5. Since there is only one major frequency, i.e., $n = 1$ in (17), the filter $G_f(s)$ can be designed as

$$G_f(s) = 1 - \frac{s(s^2 + \omega^2)}{(s+\alpha)(s^2 + \alpha_1 s + \beta_1)}. \tag{26}$$

The parameters of the filter are chosen as $\alpha = 1000$, $\alpha_1 = 1800\pi$, and $\beta_1 = 810000\pi^2$. If the tolerance of disturbance attenuation is specified as $\delta = 0.000001$, the design should satisfy $|H_d(j\omega)| \leq 20 \log \delta = -120$ dB. The error feedback gain is chosen as $k = 200\,000$. The parameters satisfy the stability condition (16). The controller is then implemented as (10). All parameters keep constant except ω in (26).

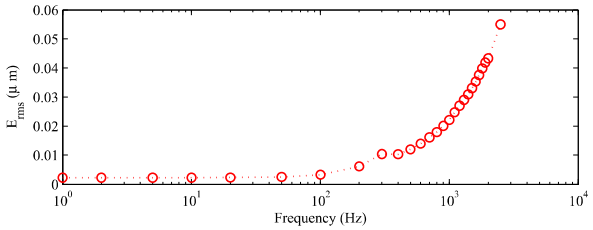

Fig. 6. Root-mean-square error when tracking sinusoidal signals with different frequencies with the proposed control scheme.

D. Experimental Results

In Fig. 6, the tracking errors $e(t) = y_m(t) - y(t)$ are shown in terms of root-mean-square (rms) error E_{rms} calculated as

$$E_{\text{rms}} = \sqrt{\frac{1}{N} \sum_{n=1}^{N} (y_m(t_n) - y(t_n))^2}$$

where N is the total number of data points, and $y_m(t_n)$ and $y(t_n)$ are the reference state and the system output at $t = t_n$, respectively. In the low-frequency range (≤ 100 Hz), the rms error is around 0.0022 μm, which is very close to the hardware resolution limit. As the frequency increases, the rms error increases, as expected. The proposed approach can track the reference signal well up to 1100 Hz, with the rms error around 0.025 μm. Fig. 7(a) and (b) depicts the tracking performance for the frequencies at 100, 500, 1000, and 1100 Hz, and Fig. 7(c) shows the Bode plots of the filters, which are designed to achieve over -120-dB attenuation of the lumped uncertainty at corresponding frequencies.

The Bode plots of the reference model (2), the open-loop system, and the closed-loop system are shown in Fig. 8. Their transfer functions are $Y_m(s)/Y_r(s)$, $Y(s)/U(s)$, and $Y(s)/Y_r(s)$, respectively. For the purpose of comparison, the results of the UDE-based state feedback controller [2] and the DOB-based controller in [2] are also presented. In [2], the UDE-based state feedback controller is derived based on the modeling of a second-order system, which requires the derivative of the system output. As seen in Fig. 8, the reference model has nearly

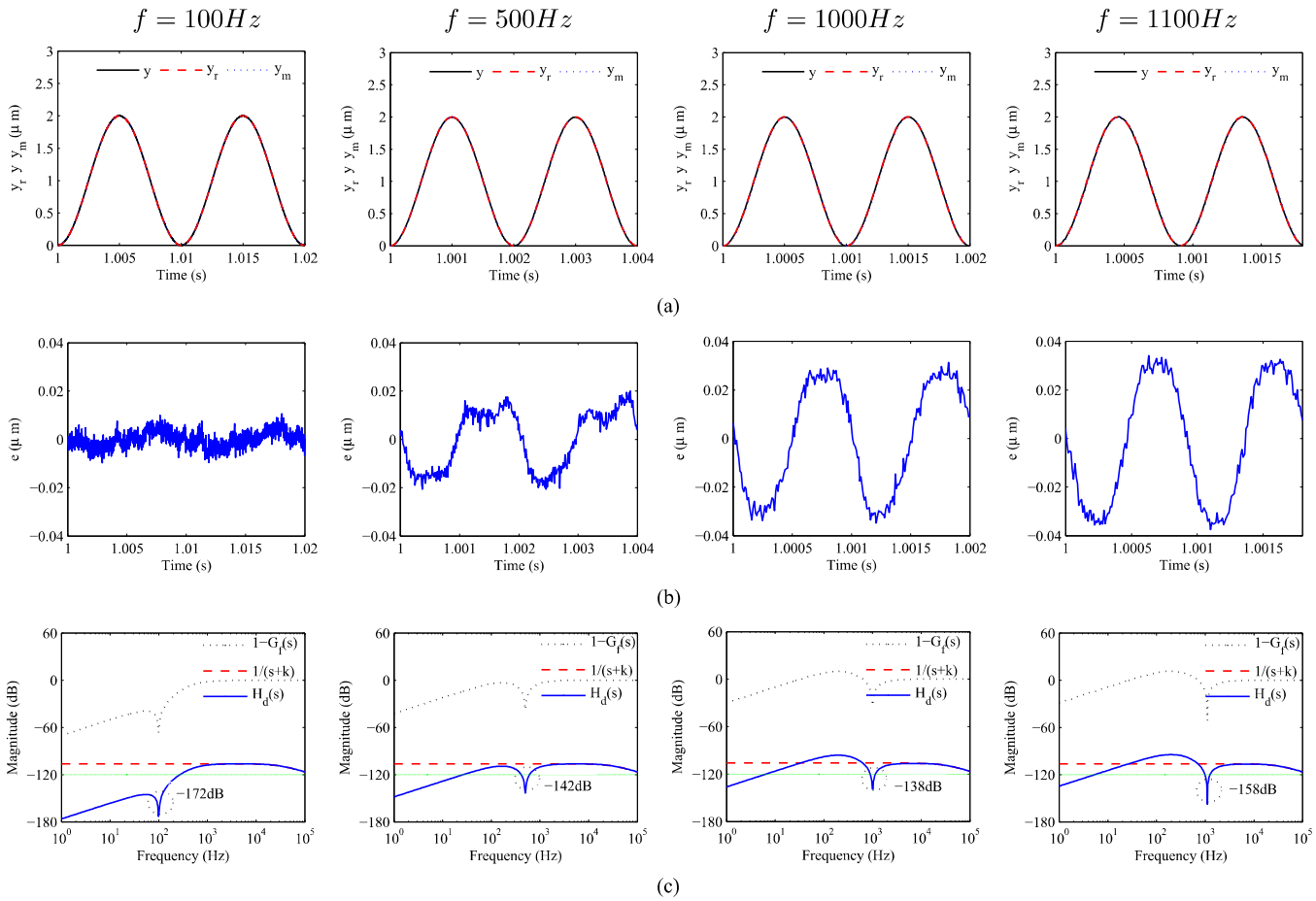

Fig. 7. Results of tracking sinusoidal signals with different frequencies. (Left to right) First column: $f = 100$ Hz; second column: $f = 500$ Hz; third column: $f = 1000$ Hz; and fourth column: $f = 1100$ Hz. (a) Output. (b) Tracking error. (c) Bode plots of $1 - G_f(s)$, $\frac{1}{s+k}$, and $H_d(s)$.

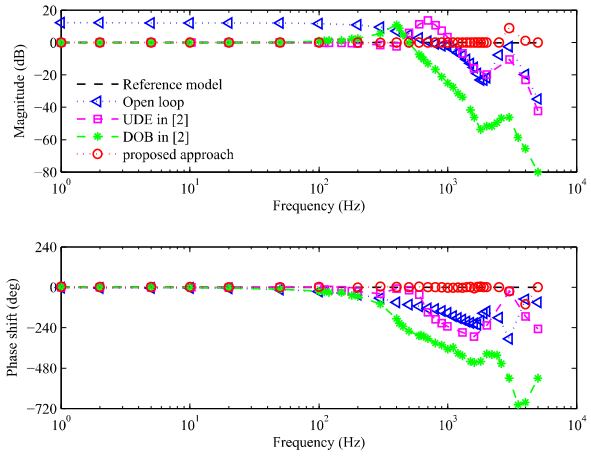

Fig. 8. Bode plots of the reference model, open-loop system, and the closed-loop system, with comparative results from [2].

TABLE II
COMPARISON OF TRACKING PERFORMANCE WITH SOME RESULTS AVAILABLE IN THE LITERATURE

Approach	Stage resonant freq.	Max tracking freq. achieved	RMS error at max freq.
Proposed approach	$2900Hz$	$1100Hz$	$0.025\mu m$
UDE in [2]	$2900Hz$	$450Hz$	$0.027\mu m$
DOB in [2]	$2900Hz$	$200Hz$	$0.577\mu m$
RAC in [24]	$2900Hz$	$100Hz$	$0.039\mu m$
PI in [34]	$1633Hz$	$510Hz$	$0.057\mu m$
DOB in [35]	$1552Hz$	$150Hz$	$0.080\mu m$
RAC in [36]	$5100Hz$	$100Hz$	$0.007\mu m$
ILC in [37]	$300Hz$	$100Hz$	$0.012\mu m$

* RAC: Robust adaptive control; ILC: Iterative learning control; PI: Proportional and integral control.

0-dB magnitude and 0° phase shift. This indicates that $Y_m(s)$ tracks $Y_r(s)$ very well. For the closed-loop system with the proposed approach, its frequency response matches the reference model in a wide range, with only one resonant peak at 3000 Hz, close to the system's first resonant frequency, 2900 Hz, which is provided in the user manual. The proposed approach can track the reference signal well up to 1100 Hz, which is much broader than the bandwidths achieved in [2]. Furthermore, the tracking bandwidth, 1100 Hz, which is 37.93% of the lowest resonant frequency, has exceeded the recommended operating frequency, 1000 Hz, provided in the user manual. In order to better illustrate the performance of the proposed approach, the results from several major works in the literature are summarized in Table II. The advantage of the proposed

approach is clear, achieving higher accuracy and wider bandwidth simultaneously.

V. Conclusion

In this article, the UDE-based robust output feedback control was proposed to remove the structural constraint and the requirement of full state measurements in the traditional UDE-based control design. The almost modeling-free feature of the proposed approach will enable more applications. The proposed approach was validated on an experimental piezoelectric nanopositioning system in the presence of hysteresis nonlinearity. Experimental results showed that high-precision and high-bandwidth trajectory tracking performance can be achieved.

References

[1] Q.-C. Zhong and D. Rees, "Control of uncertain LTI systems based on an uncertainty and disturbance estimator," *ASME Trans. J. Dyn. Syst. Meas. Control*, vol. 126, no. 4, pp. 905–910, Dec. 2004.

[2] J. Chen, B. Ren, and Q.-C. Zhong, "UDE-based trajectory tracking control of piezoelectric stages," *IEEE Trans. Ind. Electron.*, vol. 63, no. 10, pp. 6450–6459, Oct. 2016.

[3] B. Ren, Y. Wang, and Q.-C. Zhong, "UDE-based control of variable-speed wind turbine systems," *Int. J. Control*, vol. 90, no. 1, pp. 121–136, Jan. 2017.

[4] Q.-C. Zhong, Y. Wang, and B. Ren, "UDE-based robust droop control of inverters in parallel operation," *IEEE Trans. Ind. Electron.*, vol. 64, no. 9, pp. 7552–7562, Sep. 2017.

[5] L. Sun, D. Li, Q. C. Zhong, and K. Y. Lee, "Control of a class of industrial processes with time delay based on a modified uncertainty and disturbance estimator," *IEEE Trans. Ind. Electron.*, vol. 63, no. 11, pp. 7018–7028, Nov. 2016.

[6] R. Sanz, P. Garcia, Q. C. Zhong, and P. Albertos, "Predictor-based control of a class of time-delay systems and its application to quadrotors," *IEEE Trans. Ind. Electron.*, vol. 64, no. 1, pp. 459–469, Jan. 2017.

[7] Q. Lu, B. Ren, S. Parameswaran, and Q.-C. Zhong, "UDE-based robust trajectory tracking control for a quadrotor in a GPS-denied environment," *ASME Trans. J. Dyn. Syst. Meas. Control*, vol. 140, no. 3, Mar. 2018, Art. no. 031001.

[8] J. P. Kolhe, M. Shaheed, T. S. Chandar, and S. E. Talole, "Robust control of robot manipulators based on uncertainty and disturbance estimation," *Int. J. Robust Nonlinear Control*, vol. 23, no. 1, pp. 104–122, Jan. 2013.

[9] J. Dai and B. Ren, "UDE-based robust boundary control for an unstable parabolic PDE with unknown input disturbance," *Automatica*, vol. 93, pp. 363–368, Jul. 2018.

[10] Q.-C. Zhong, A. Kuperman, and R. Stobart, "Design of UDE-based controllers from their two-degree-of-freedom nature," *Int. J. Robust Nonlinear Control*, vol. 21, pp. 1994–2008, Nov. 2011.

[11] B. Ren, Q.-C. Zhong, and J. Dai, "Asymptotic reference tracking and disturbance rejection of UDE-based robust control," *IEEE Trans. Ind. Electron.*, vol. 64, no. 4, pp. 3166–3176, Apr. 2017.

[12] J. Dai, B. Ren, and Q.-C. Zhong, "Uncertainty and disturbance estimator-based backstepping control for nonlinear systems with mismatched uncertainties and disturbances," *ASME Trans. J. Dyn. Sys. Meas. Control*, vol. 140, no. 12, Dec. 2018, Art. no. 121005.

[13] S. Talole, T. Chandar, and J. P. Kolhe, "Design and experimental validation of UDE based controller–observer structure for robust input–output linearisation," *Int. J. Control*, vol. 84, no. 5, pp. 969–984, Jun. 2011.

[14] J. Yang, S. Li, and X. Yu, "Sliding-mode control for systems with mismatched uncertainties via a disturbance observer," *IEEE Trans. Ind. Electron.*, vol. 60, no. 1, pp. 160–169, Jan. 2012.

[15] A. Levant, "Higher-order sliding modes, differentiation and output-feedback control," *Int. J. Control*, vol. 76, nos. 9/10, pp. 924–941, Nov. 2003.

[16] J. Yao, Z. Jiao, and D. Ma, "Extended-state-observer-based output feedback nonlinear robust control of hydraulic systems with backstepping," *IEEE Trans. Ind. Electron.*, vol. 61, no. 11, pp. 6285–6293, Nov. 2014.

[17] J. Yao and W. Deng, "Active disturbance rejection adaptive control of hydraulic servo systems," *IEEE Trans. Ind. Electron.*, vol. 64, no. 10, pp. 8023–8032, Oct. 2017.

[18] B. Mirkin and P.-O. Gutman, "Robust output-feedback model reference adaptive control of SISO plants with multiple uncertain, time-varying state delays," *IEEE Trans. Autom. Control*, vol. 53, no. 10, pp. 2414–2419, Nov. 2008.

[19] B. Ren, Q.-C. Zhong, and J. Chen, "Robust control for a class of non-affine nonlinear systems based on the uncertainty and disturbance estimator," *IEEE Trans. Ind. Electron.*, vol. 62, no. 9, pp. 5881–5888, Sep. 2015.

[20] K. K. Leang, Q. Zou, and S. Devasia, "Feedforward control of piezoactuators in atomic force microscope systems," *IEEE Control Syst. Mag.*, vol. 29, no. 1, pp. 70–82, Feb. 2009.

[21] D. Wang, Q. Yang, and H. Dong, "A monolithic compliant piezoelectric-driven microgripper: Design, modeling, and testing," *IEEE/ASME Trans. Mechatronics*, vol. 18, no. 1, pp. 138–147, Sep. 2013.

[22] G. M. Clayton, S. Tien, K. K. Leang, Q. Zou, and S. Devasia, "A review of feedforward control approaches in nanopositioning for high-speed SPM," *J. Dyn. Syst., Meas. Control*, vol. 131, no. 6, Oct. 2009, Art. no. 061101.

[23] J. Y. Peng and X. B. Chen, "Integrated PID-based sliding mode state estimation and control for piezoelectric actuators," *IEEE/ASME Trans. Mechatronics*, vol. 19, no. 1, pp. 88–99, Feb. 2014.

[24] G.-Y. Gu, L.-M. Zhu, C.-Y. Su, and H. Ding, "Motion control of piezoelectric positioning stages: Modeling, controller design, and experimental evaluation," *IEEE/ASME Trans. Mechatronics*, vol. 18, no. 5, pp. 1459–1471, Oct. 2013.

[25] A. Al-Mamun, E. Keikha, C. S. Bhatia, and T. H. Lee, "Integral resonant control for suppression of resonance in piezoelectric micro-actuator used in precision servomechanism," *Mechatronics*, vol. 23, no. 1, pp. 1–9, Feb. 2013.

[26] L. Liu, K. K. Tan, and T. H. Lee, "Multirate-based composite controller design of piezoelectric actuators for high-bandwidth and precision tracking," *IEEE Trans. Control Syst. Technol.*, vol. 22, no. 2, pp. 816–821, Mar. 2014.

[27] J. Dai, B. Ren, and Q.-C. Zhong, "Output feedback trajectory tracking control via uncertainty and disturbance estimator," in *Proc. American Control Conf.*, Milwaukee, WI, USA, Jun. 2018, pp. 2139–2144.

[28] H. K. Khalil, *Nonlinear Systems*. Englewood Cliffs, NJ, USA: Prentice-Hall, 2001.

[29] M. Al Janaideh and P. Krejci, "Inverse rate-dependent Prandtl–Ishlinskii model for feedforward compensation of hysteresis in a piezomicropositioning actuator," *IEEE/ASME Trans. Mechatronics*, vol. 18, no. 5, pp. 1498–1507, Oct. 2013.

[30] M. Al Janaideh, S. Rakheja, and C.-Y. Su, "Experimental characterization and modeling of rate-dependent hysteresis of a piezoceramic actuator," *Mechatronics*, vol. 19, no. 5, pp. 656–670, Aug. 2009.

[31] R. Ben Mrad and H. Hu, "A model for voltage-to-displacement dynamics in piezoceramic actuators subject to dynamic-voltage excitations," *IEEE/ASME Trans. Mechatronics*, vol. 7, no. 4, pp. 479–489, Dec. 2002.

[32] G. Gu and L. Zhu, "Modeling of rate-dependent hysteresis in piezoelectric actuators using a family of ellipses," *Sens. Actuators A, Phys.*, vol. 165, no. 2, pp. 303–309, Feb. 2011.

[33] M. Al Janaideh, S. Rakheja, and C.-Y. Su, "An analytical generalized Prandtl–Ishlinskii model inversion for hysteresis compensation in micropositioning control," *IEEE/ASME Trans. Mechatronics*, vol. 16, no. 4, pp. 734–744, Aug. 2011.

[34] M.-J. Yang, G.-Y. Gu, and L.-M. Zhu, "High-bandwidth tracking control of piezo-actuated nanopositioning stages using closed-loop input shaper," *Mechatronics*, vol. 24, no. 6, pp. 724–733, Sep. 2014.

[35] J. Yi, S. Chang, and Y. Shen, "Disturbance-observer-based hysteresis compensation for piezoelectric actuators," *IEEE/ASME Trans. Mechatronics*, vol. 14, no. 4, pp. 456–464, Aug. 2009.

[36] J. Zhong and B. Yao, "Adaptive robust precision motion control of a piezoelectric positioning stage," *IEEE Trans. Control Syst. Technol.*, vol. 16, no. 5, pp. 1039–1046, Sep. 2008.

[37] D. Huang, J.-X. Xu, V. Venkataramanan, and T. C. T. Huynh, "High-performance tracking of piezoelectric positioning stage using current-cycle iterative learning control with gain scheduling," *IEEE Trans. Ind. Electron.*, vol. 61, no. 2, pp. 1085–1098, Feb. 2013.

Beibei Ren (S'05–M'10) received the B.Eng. degree in mechanical and electronic engineering and the M.Eng. degree in automation from Xidian University, Xi'an, China, in 2001 and 2004, respectively, and the Ph.D. degree in the electrical and computer engineering from the National University of Singapore, Singapore, in 2010.

From 2010 to 2013, she was a Postdoctoral Scholar with the Department of Mechanical and Aerospace Engineering, University of California, San Diego, CA, USA. She is currently an Associate Professor with the Department of Mechanical Engineering, Texas Tech University, Lubbock, TX, USA. Her current research interests include robust control theory and its application to mechatronics, and renewable energy systems.

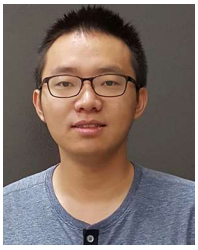

Jiguo Dai (S'15) received the B.Eng. degree in thermal energy and power engineering from Northwestern Polytechnical University, Xi'an, China, in 2013, and the Ph.D. degree in mechanical engineering from Texas Tech University, Lubbock, TX, USA, in 2019.

His current research interests include robust control theory and applications in servo systems.

Qing-Chang Zhong (M'04–SM'04–F'17) received two Ph.D. degrees, one in control and power engineering from Imperial College London, London, U.K., in 2004, and the other in control theory and engineering from Shanghai Jiao Tong University, Shanghai, China, in 2000.

He holds the Max McGraw Endowed Chair Professor in Energy and Power Engineering with the Department of Electrical and Computer Engineering, Illinois Institute of Technology, Chicago, IL, USA. He is the Founder & CEO of Syndem LLC, Chicago. He spent nearly 15 years in the U.K. and was the Chair Professor of Control and Systems Engineering with the University of Sheffield before moving to Chicago. He proposed the synchronized and democratized smart grid architecture to unify the integration of nonsynchronous distributed energy resources and flexible loads. He is the (co)author of four research monographs.

Dr. Zhong serves/served as a Steering Committee Member for the IEEE Smart Grid, a Distinguished Lecturer for the IEEE Power Electronics Society, the IEEE Control Systems Society, the IEEE Power and Energy Society, an Associate Editor for the IEEE TRANSACTIONS ON AUTOMATIC CONTROL, IEEE TRANSACTIONS ON INDUSTRIAL ELECTRONICS, IEEE TRANSACTIONS ON POWER ELECTRONICS, IEEE TRANSACTIONS ON CONTROL SYSTEMS TECHNOLOGY, IEEE ACCESS, IEEE JOURNAL OF EMERGING AND SELECTED TOPICS IN POWER ELECTRONICS, and a Vice-Chair for International Federation of Automatic Control Technical Committee on Power and Energy Systems. He was a Senior Research Fellow of the Royal Academy of Engineering, U.K., and the U.K. Representative to European Control Association.